Citation: CPT Pharmacometrics Syst. Pharmacol. (2015) 4, e13; doi:10.1002/psp4.13

ORIGINAL ARTICLE

Physiologically Based Pharmacokinetic Modeling of Fluorescently Labeled Block Copolymer Nanoparticles for Controlled Drug Delivery in Leukemia Therapy

MJ Gilkey[1], V Krishnan[2,3], L Scheetz[4], X Jia[2,4,5], AK Rajasekaran[2,5,6] and PS Dhurjati[1]*

A physiologically based pharmacokinetic (PBPK) model was developed that describes the concentration and biodistribution of fluorescently labeled nanoparticles in mice used for the controlled delivery of dexamethasone in acute lymphoblastic leukemia (ALL) therapy. The simulated data showed initial spikes in nanoparticle concentration in the liver, spleen, and kidneys, whereas concentration in plasma decreased rapidly. These simulation results were consistent with previously published *in vivo* data. At shorter time scales, the simulated data predicted decrease of nanoparticles from plasma with concomitant increase in the liver, spleen, and kidneys before decaying at longer timepoints. Interestingly, the simulated data predicted an unaccounted accumulation of about 50% of the injected dose of nanoparticles. Incorporation of an additional compartment into the model justified the presence of unaccounted nanoparticles in this compartment. Our results suggest that the proposed PBPK model can be an excellent tool for prediction of optimal dose of nanoparticle-encapsulated drugs for cancer treatment.
CPT Pharmacometrics Syst. Pharmacol. (2015) **4**, e13; doi:10.1002/psp4.13; published online on 12 March 2015.

Physiologically based pharmacokinetic (PBPK) models provide a means by which one can predict the biodistribution of a drug in the body over time.[1–3] *In vivo* animal studies are used to develop an initial PBPK model and make the correct assumptions about important organs and the connectivity of the system.[4] Critical assumptions include (a) selection of organs to incorporate in the model, (b) the connectivity among these organs via blood flow, (c) the partitioning of the drug between the tissue and vascular compartments, and (d) other physiological parameters.[1–4] The initial PBPK mouse model can later be adapted to describe the drug distribution in humans.[4,5] Simulations with PBPK models provide insight on appropriate dosage regimens to be used.[6,7] Since the Bischoff model, many drugs have been physiologically modeled with success.[1,4,8–10]

Nanoparticle-mediated drug delivery introduces additional complexities in drug biodistribution. The distribution of the drug may depend on the encapsulating material and size of the nanoparticles.[11] Therefore, it is important to monitor the biodistribution of nanoparticles to better understand the biodistribution of the encapsulated drug.[12–16] PBPK modeling could potentially be a promising approach to predict biodistribution trends in humans before clinical trials because initial predictions are made based on the actual distribution of nanoparticles in preclinical mouse models.[5] However, such modeling systems for specific nanoparticle-based drug delivery are not well developed.

Studies pertaining to dexamethasone-encapsulated nanoparticles (Dex-NPs) generated for drug delivery in acute lymphoblastic leukemia (ALL) therapy were used for modeling.[17] ALL is a cancer of the blood and has been known to affect primarily children and adolescents. Dex belongs to the glucocorticoid class of steroid hormones and is widely used in combination with other chemotherapeutic agents to treat ALL.[18] The drug, however, induces cytotoxicity in normal lymphocytes and triggers deleterious side effects because of prolonged systemic exposure.[19] Some of the most commonly observed treatment-related side effects of Dex include edema, increase in body weight, damage to joints resulting in pain, and restricted motion that may involve the hip and knee (osteoporosis), high blood sugar (Cushing syndrome), high blood pressure (hypertension), and, most important, the drug weakens the body's immune system because of indiscriminate killing of normal B and T lymphocytes, thereby causing immunosuppression in children.[20]

In this study, we utilized fluorescently labeled nanoparticles as a surrogate for Dex-NPs and extended the PBPK modeling approach to predict relative concentrations of nanoparticles in various organs. This system has been vigorously validated previously and was shown to improve survival and reduce disease symptoms in mice with leukemia.[17] The modeling of nanoparticle biodistribution is based on physiological phenomena interrelating flow rates, distribution ratios, rate constants, and elimination rates in mice or other animal models. Using data gathered from nanoparticle accumulation in mice, key physiological parameters were determined to construct a PBPK model for these nanoparticles.

RESULTS

A model was developed that accurately depicts the biodistribution of the nanoparticle in the body as a function of time at shorter (up to 2 days; **Figures 1 and 2**) and extended time intervals (up to 14 days; **Figure 3**). Simulations were created using the experimental data obtained by intravenous injection of 5 mcg/mL of 1,1′-Dioctadecyl-

[1]Department of Chemical and Biomolecular Engineering, University of Delaware, Newark, Delaware, USA; [2]Department of Materials Science and Engineering, University of Delaware, Newark, Delaware, USA; [3]Nemours Biomedical Research, A I DuPont Hospital for Children, Wilmington, Delaware, USA; [4]Department of Biomedical Engineering, University of Delaware, Newark, Delaware, USA; [5]Department of Biological Sciences, Center for Translational Cancer Research, University of Delaware, Newark, Delaware, USA; [6]Lankenau Institute for Medical Research, Wynnewood, Pennsylvania, USA. *Correspondence: PS Dhurjati (dhurjati@udel.edu)
Received 7 July 2014; accepted 9 November 2014; published online on 12 March 2015. doi:10.1002/psp4.13

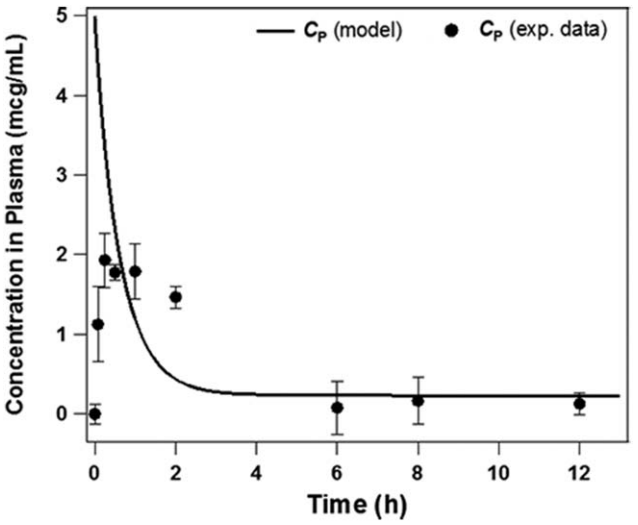

Figure 1 Concentration profile of nanoparticles in the plasma vs. time over all timepoints. The solid circles denote experimental data, and the continuous curve represents the simulated data. Note the good agreement between experimental data and predicted model at $t < 2$ hours and $t > 6$ hours.

3,3,3′,3′-Tetramethylindotricarbocyanine Iodide dye-encapsulated nanoparticles (DiR-NPs), as described previously.[17] In **Figure 1**, the experimental data provided suggests that there exists a lag between initial injection and uptake in the plasma (t ~0–4 hours). The model, however, treats the injection as a step input, whereas at $t = 0$ all of the injected nanoparticles are contained in the plasma (5 mcg/mL) and undergo an exponential decay as expected. Although discrepancy exists at $t = 0$, the predicted plasma concentration accurately demonstrates the time scale of clearance of nanoparticles from the blood into other organs. After about an hour, there is good agreement in that roughly 40% of the injected dose of DiR-NPs has cleared from the plasma, and after 6 hours, nearly all DiR-NPs have left the plasma, as revealed by both the experimental data and the model.

Figure 2 shows the short time distribution (up to 48 hours) of DiR-NPs in the organs, such as liver, spleen, and kidneys. The experimental data from imaging of harvested tissues revealed nanoparticle accumulation in the liver (1.10–1.58 mcg/mL), spleen (0.22–0.3 mcg/mL), and kidneys (0.28–0.52 mcg/mL). Fluorescence was not detected in any other organs.[17] The model predicts accumulation of DiR-NPs in the liver, spleen, and kidneys increases shortly after intravenous injection until a maximum is reached (peak plasma concentration $[C_{max}]_L$ ~1.7 mcg/mL, $C_{max,S}$ ~0.5 mcg/mL, and $C_{max,K}$ ~1.7 mcg/mL) and clearance of nanoparticles begins ($t_{max,L}$ ~2.6 hours, $t_{max,S}$ ~0.5 hours, $t_{max,K}$ ~0.5 hours) subsequently. The range of experimental values was close to the predicted values at this time scale (**Supplementary Table S1**). In the liver, at $t = 2$ hours, there exists a deviation of about 0.6 mcg/mL DiR-NPs between the simulated and actual data obtained in mice; however, this difference is still maintained within the experimental error.

Figure 3 shows the model at longer time scales (up to 14 days). The experimental data revealed clearance of nanoparticles in the liver (1.58–0.28 mcg/mL), spleen (0.30–0.12

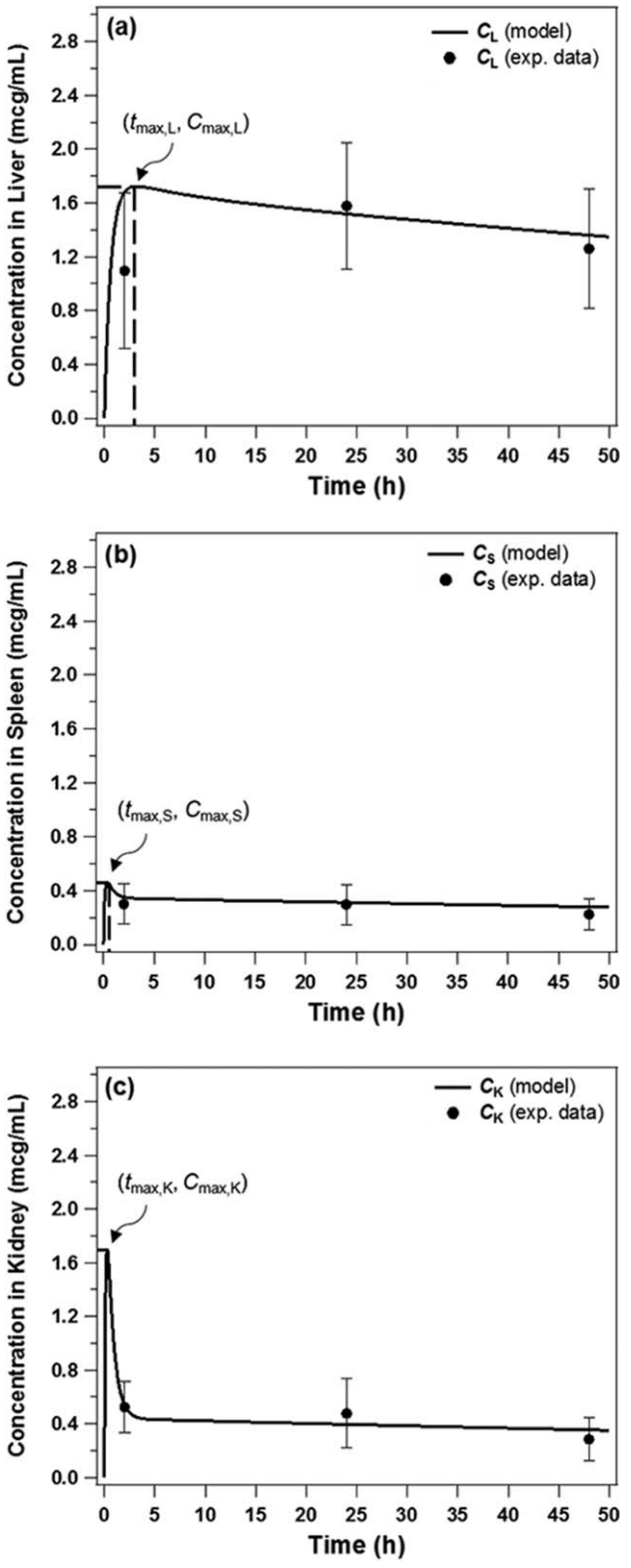

Figure 2 Biodistribution data and physiologically based pharmacokinetic (PBPK) nanoparticle model on short time scale (up to 48 hours) including the: (**a**) liver, (**b**) spleen, and (**c**) kidneys. The solid circles denote experimental data, and the continuous curve represents the simulated data. Note the close fit between experimental values and predicted values. A small deviation (0.6 mcg/mL) of 1,1′-Dioctadecyl-3,3,3′,3′-Tetramethylindotricarbocyanine Iodide dye-encapsulated nanoparticles (DiR-NPs) that exists between simulated and actual data is within the experimental error.

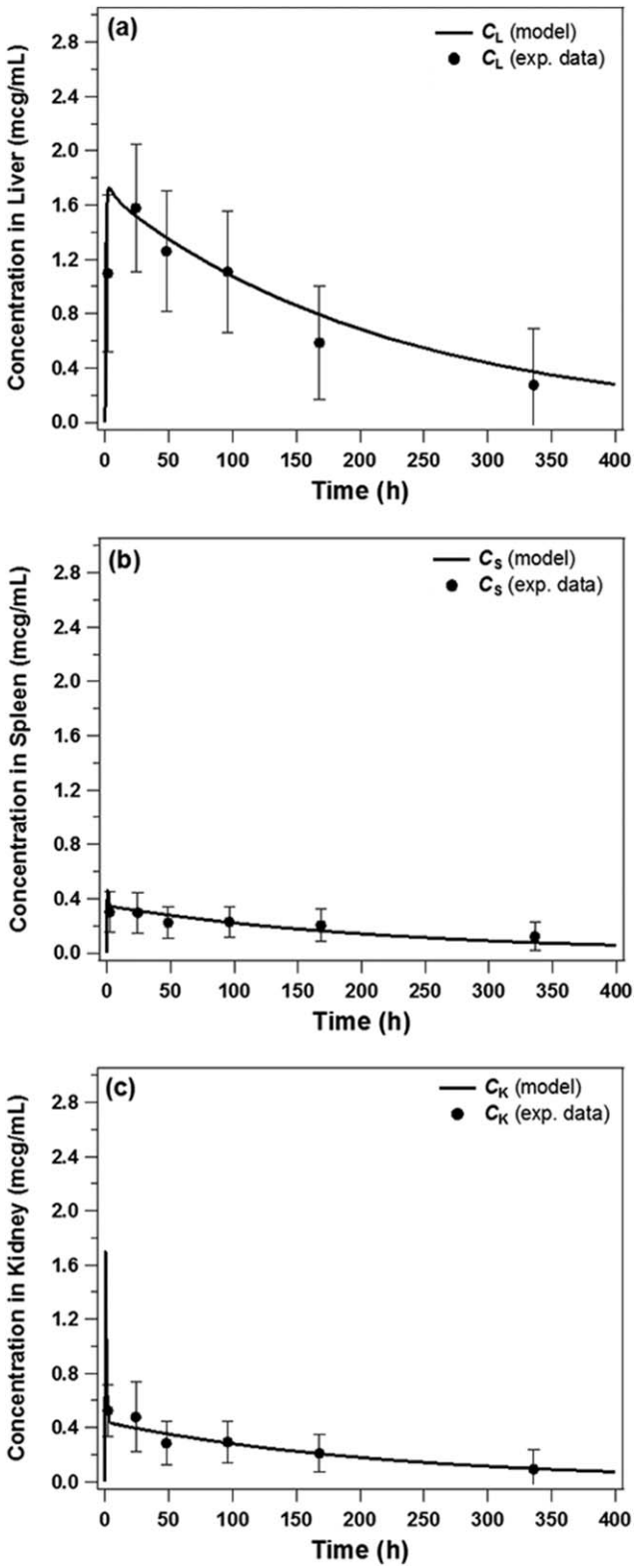

Figure 3 Biodistribution data and physiologically based pharmacokinetic (PBPK) nanoparticle model on long time scale (up to 14 days) including the: (**a**) liver, (**b**) spleen, and (**c**) kidneys. The solid circles denote experimental data, and the continuous curve represents the simulated data. Note the perfect fit between experimental and simulated values.

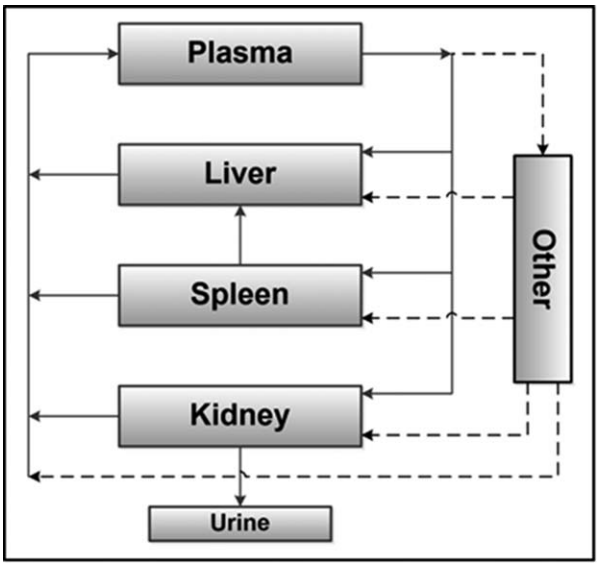

Figure 4 Flow diagram of the compartmentalized model. Note inclusion of a virtual organ referred to as the "other" compartment, and denoted "o" incorporated into the model.

mcg/mL), and kidneys (0.52–0.09 mcg/mL).[17] The predicted values were strikingly similar to experimental values, and the predicted curve aligned perfectly with the observed values at each timepoint (**Supplementary Table S1**).

Although 5 mcg/mL was injected, the experimental data could account for only about 50% of the administered dose. To explain the remaining 50% of nanoparticles injected, a virtual compartment designated as "other" compartment was incorporated into the model (**Figure 4**). The model prediction of the concentration profile of the "other" compartment reveals that the theoretical understanding of this organ is consistent with its simulated features. Shortly after the step input at $t = 0$ hours, the concentration rises suddenly with the decrease of DiR-NPs in the plasma (**Figure 5a** compared with **Figure 1**). After reaching a maximum ($t_{max,O} \sim 3$ hours, $C_{max,O} \sim 2.6$ mcg/mL), the concentration decays gradually as nanoparticles in the "other" compartment and the liver, spleen, and kidneys begin to clear (**Figure 5b**). It is important to note that the characteristic time scale of nanoparticle depletion in each organ is qualitatively similar after C_{max} is reached ($t_{1/2} \sim 100$ hours). Thus, it can be concluded that the discrepancy in the mass balance was accounted for by the introduction of this additional compartment. Although the compartment cannot be identified precisely except through speculation, its properties can be physically and theoretically justified (see Discussion).

We analyzed measurement variability by a sensitivity analysis technique by perturbing each estimated parameter by 20%, which showed that the equilibrium constant in the "other" organ, R_O (**Figure 6a**), the kidney clearance, K_K (**Figure 6b**), and the equilibrium constant between the kidneys and the "other" organ, R_{KO} (**Figure 6c**), were very sensitive to small perturbations in the estimated value. In particular, perturbations can cause mathematical divergence in the response curves. For example, by increasing R_O by 20% to 12.06 and keeping all other parameters

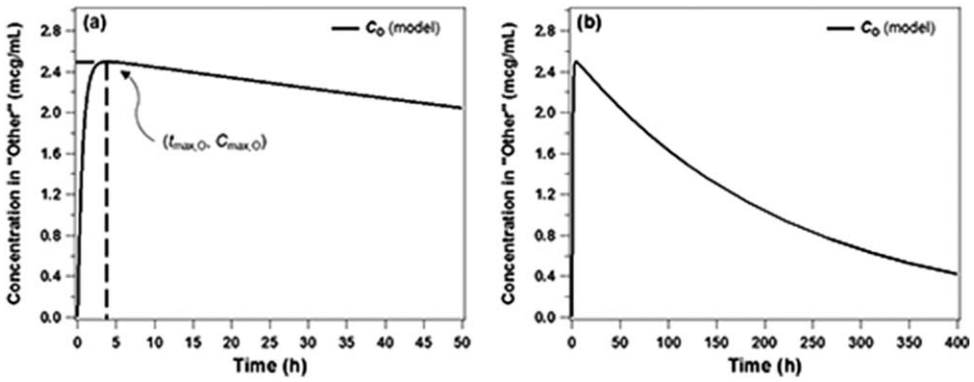

Figure 5 Biodistribution data and physiologically based pharmacokinetic (PBPK) nanoparticle model on short and long time scale for the "other" compartment or "o." Note the sudden increase in the 1,1′-Dioctadecyl-3,3,3′,3′-Tetramethylindotricarbocyanine Iodide dye-encapsulated nanoparticle (DiR-NP) concentration at the shorter time scale (**a**) and exponential decay at the longer time scale (**b**).

constant, the concentration in the liver diverges after about 20 hours; however, decreasing R_O has no significant impact on the uptake in the organs of interest (**Figure 6**). Similar observations were noted by perturbing K_K and R_{KO}. Mathematically, this implies that these parameters must be uniquely defined to maintain stability in the response.

DISCUSSION

The largest differences between the predicted value and the experimental data occur in the plasma from $t = 0$–2 hours. The particles were injected via the tail vein and blood was drawn from the submandibular region starting at 0.08 hours (5 minutes). It is important to take into consideration the diffusive transport rate of nanoparticles from the site of injection to the whole body. At 0.08 hours, the levels of nanoparticles detected in the blood were low because the particles were only partially distributed throughout the body. Therefore, at 0.08 hours, the experimental data is less significant because the model does not account for partial distribution or time-dependent adsorption of nanoparticles. Further, the experimental data indicates that at 0.25 hours, the diffusible nanoparticles are distributed throughout the whole body. Nevertheless, the predicted value is a fold higher than the experimental value at earlier time points ($t =$ 0–2 hours). This may be due to the aggregation of nanoparticles in the blood, their adsorption to the endothelial walls, and subsequent release resulting in differences between the experimental and predicted levels of nanoparticles in the blood. The model takes into account the entire injected dose from the syringe and does not account for the aggregated, adsorbed, or released nanoparticles. Nonetheless, the model effectively predicts the length of time nanoparticles remain in the body in each organ, which is of greater importance in designing dosage regimes.

With regard to the existence of the "other" compartment, a possible explanation pertains to the adsorption of DiR-NPs to the endothelial walls of blood vessels. This is the tissue that comes into contact with the nanoparticles immediately after intravenous administration. It is documented that over 50% higher particle binding to the vessel wall was observed when the motion and adhesion of individual nanoparticles are tracked through Brownian adhesion dynamics.[21] If adhesion of nanoparticles to the endothelial walls does adsorb nanoparticles shortly after the injection, the accumulation in the other organ should reflect the numbers observed in Tan *et al*.[21] The simulations in **Figures 1–3** were conducted with an injection of 5 mcg/mL. The maximum value in the "other" organ shows a value of ~2.5 mcg/mL in **Figure 3**, which is approximately 50% of the injection. Therefore, the mathematical prediction made by the model agrees very closely with the biological data, thereby substantiating the physical meaning of the model. Another potential "other" compartment is the lymphatic system. Plasma components readily move across blood vessels into lymphatic tissue, causing some exchange between the lymph and plasma. In this case, accumulation and binding of nanoparticles to lymphatic tissue is plausible to explain for unaccounted accumulation resulting in discrepancy between the model and the actual data. Because lymphatic tissue is found virtually all throughout the body, its anatomic locations proximal to the spleen, liver, and kidneys make the lymphatic system a reasonable one to which to attribute the "other" compartment.[21,22]

Exchange between the established PBPK compartments and the new compartment for the blood vessel wall, and possibly the lymph, may justify the DiR-NPs accumulation previously unrecognized. The rapid drop in nanoparticle concentration after injection and the steadily low nanoparticle concentration in the plasma and its accumulation in the other organs are likely resultant of these phenomena. Although this justification for the nanoparticle accumulation discrepancy is physiologically sensible, all of the discrepancy cannot be attributed only to the above tissues.

To create better agreement between the model and experiments, the volumetric flow rate of plasma through the liver (Q_L) was estimated. Although this parameter is typically treated as a physiologically predetermined parameter, we hypothesize its estimation is justified because of incorporating so few physiological compartments into the model. Because of this, the plasma flow rate through the liver took up a larger percent of the total plasma flow rate represented in the model. From a mathematical perspective, this creates large overshoots in initial concentration of

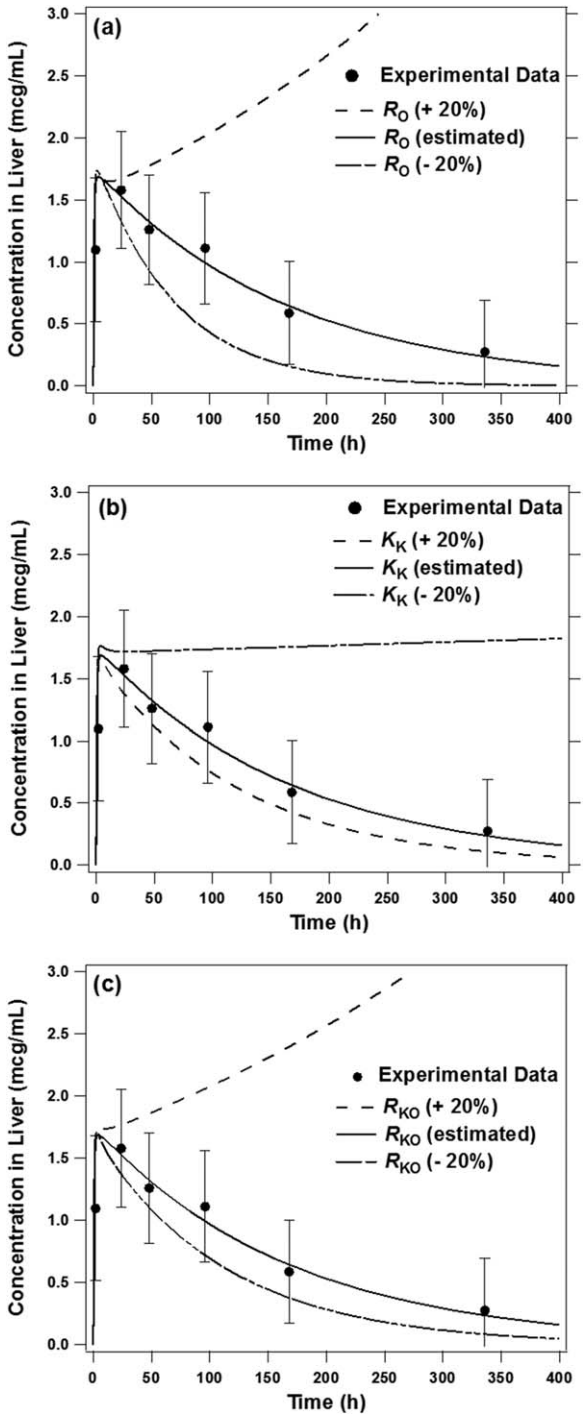

Figure 6 Sensitivity analysis showing the effect of perturbing R_O by ±20%. The solid circles denote experimental data and the continuous lines represent the simulated data. The broken and the partially broken lines denote change in 1,1′-Dioctadecyl-3,3,3′,3′-Tetramethylindotricarbocyanine Iodide dye-encapsulated nanoparticle (DiR-NP) concentration by perturbations of each parameter by ±20%, respectively. The plots **a**, **b**, and **c** show the sensitivity of the DiR-NP concentration in the liver to perturbation for three different parameters. Each parameter was perturbed by ±20% and their effect on the liver concentration is shown. Note that the sensitivity of the concentration in the liver causes instability beyond experimentally determined error for each parameter.

nanoparticles in the liver beyond the experimental uncertainty, which does not describe the experimental data.

The sensitivity analysis revealed that biologically significant parameters must be uniquely defined to avoid incorrect model predictions or mathematical instability. Each sensitive parameter (R_O, K_K, and R_{KO}) included some interaction with the kidneys. If everything else is constant, this indicates that nanoparticle accumulation in the kidneys and its subsequent clearance plays an important role in the model.

Fluorescent dye and Dex-NPs are made up of the same material (i.e., amphiphilic block copolymers consisting of hydrophilic polyethylene glycol and hydrophobic polyester bearing pendant cyclic ketals) and possess identical physicochemical properties.[17] The difference is in the payload: Dex-NPs contain Dex, and fluorescent DiR-NPs contain DiR. Further, the dose injected for DiR-NPs is comparable to the 5 mcg/mL dose of Dex-NPs administered.[17] Therefore, the focus is upon the distribution of the carrier nanoparticles and not the payload. This suggests that the biodistribution of DiR-NPs used in our modeling should mimic a similar pharmacokinetic behavior for Dex-NPs used in our preclinical study.[17]

Nanoparticles typically accumulate rapidly in the liver and spleen.[20] This may be an advantage in the treatment of ALL. The liver and spleen are sites for leukemia blast accumulation and proliferation. This results in enlargement and inflammation of these organs, causing hepatosplenomegaly, a symptom in pediatric ALL.[23] As predicted by the model and in agreement with the previous biodistribution data, it takes more than 2 weeks for DiR-NPs to be cleared from the tissues. This suggests that Dex-NPs are available for extended periods as a controlled release system supplying the drug needed to curb leukemia progression. This might have resulted in significantly reduced disease symptoms and improved survival of ALL-bearing mice reported earlier. It is known that the size of nanoparticles plays a significant role in its half-life in the plasma.[20] In contrast to nanoparticles larger than 100 nm, small-sized nanoparticles circulate longer on account of not being cleared by the macrophage phagocytic system. It may be interesting to include biodistribution data obtained from differentially sized nanoparticles in our modeling approach to predict both short- and long-term behavior of particles in biological systems. Subsequently, modeling for Dex-NPs and possibly other drug-encapsulated nanoparticles can be useful in developing an optimal regimen for children with ALL.

METHODS AND THEORETICAL BACKGROUND

In vivo plasma pharmacokinetics and organ biodistribution studies

In vivo studies and pharmacokinetics were performed as described previously.[17] Briefly, for evaluating plasma pharmacokinetics, 100 μl of DiR dye-encapsulated nanoparticles (5 mcg/mL) resuspended in phosphate-buffered saline was injected intravenously into female BALB/c mice (4–6 weeks of age; 3 per group). Peripheral blood was then collected from mice by submandibular bleeding in tubes containing 20 μl of sodium citrate to prevent blood from clogging at the indicated timepoints. Plasma was isolated by centrifugation and DiR fluorescence levels were measured using a multilabel microplate

reader (Plate Chameleon V, Hidex, Finland). The values obtained were then compared with standards prepared in plasma to obtain the appropriate nanoparticle levels.

To study organ biodistribution and clearance of DiR-NPs, female BALB/c mice (4–6 weeks of age; 3 per group) were intravenously administered with a single dose of 100 μl of DiR-NPs (5 mcg/mL). Organs, such as the liver, spleen, heart, lungs, kidneys, intestine, gonads, bladder, and brain, were harvested from mice euthanized at the indicated timepoints. The dissected organs were then imaged using the Carestream Multi-spectral *in vivo* Imaging System. Subsequently, DiR-NPs were extracted from the organs in tissue lysis buffer (20 m*M* Tris-HCL, pH 7.5; 150 m*M* sodium chloride; 1 m*M* EDTA; 1 m*M* EGTA; 1 m*M* β-glycerol phosphate; 1 m*M* sodium vanadate; 2.5 m*M* sodium pyrophosphate; 1% [w/v] triton X-100; 1% [w/v] IGEPAL; 0.5% [w/v] deooxycholate; 1% [w/v] sodium dodecyl sulfate) and 1% protease inhibitor cocktail (100 m*M* phenylmethylsulfonyl fluoride, 1:100; 15 mg/mL mixture of antipain, leupeptin, pepstatin, 1:1000; Sigma-Aldrich, St. Louis, MO) at 4°C for 1 hour. Finally, the DiR-NP fluorescence levels in the tissue lysates were measured using Carestream's image analysis software, and values obtained were compared with standards prepared in tissue lysis buffer. BALB/c mice injected with saline were included as experimental controls, and organs harvested from this group were used as background to establish the settings for DiR-NP fluorescence analysis. *In vivo* experiments were performed in accordance with protocols and guidelines approved by the Institutional Animal Care and Use Committee.

Initial data analysis and assumptions

Data were collected showing the concentration of nanoparticles as a function of time in various organs in mice.[17] Measurement of nanoparticles was conducted by encapsulating a fluorescent dye DiR from which quantitative data was collected in percent of injected dose at various time increments in the body. It was observed that fluorescent nanoparticles accumulated only in four organs in mice: the plasma, the liver, the kidneys, and the spleen.[17] Because no fluorescence was detected elsewhere, the mathematical model must initially assume that no nanoparticle accumulation occurred elsewhere in the body.

The Bischoff model[1,4] was used as a basis for constructing the mathematical model to predict the PBPK of these nanoparticles. Each of the selected organs was modeled as a continuous-stirred tank reactor, and several predetermined physiological constants were incorporated, such as volumetric blood flow rates through the organ, volume of the organ, etc. It is important to note that absorption of the nanoparticles in the organ was modeled via equilibrium constants. No kinetic absorption was considered, because it is assumed that absorption is thermodynamically limited rather than rate-limited as in Bischoff's model.[1]

Using a simple mass balance, the general equation, which describes the accumulation of nanoparticles in each organ, is described in Eq. 1.

$$\begin{aligned}[\text{rate of NP accumulation}] = {} & [\text{rate of NP in}] - [\text{rate of NP out}] \\ & - [\text{rate of NP clearance}] \\ & + [\text{rate of NP absorption}]\end{aligned} \tag{1}$$

Using Eq. 1 to develop mass balances for each of the four compartments, the following equations can be derived:

$$\text{Plasma} \quad \frac{dC_P}{dt} = \frac{1}{V_P}\left[\left(\frac{C_L}{R_L}Q_L + \frac{C_S}{R_S}Q_S + \frac{C_K}{R_K}Q_K\right) - C_P(Q_L + Q_S + Q_K)\right] \tag{2}$$

$$\text{Liver} \quad \frac{dC_L}{dt} = \frac{1}{V_L}\left[\left(C_P(Q_L - Q_S) + \frac{C_S}{R_S}Q_S\right) - \frac{C_L}{R_L}Q_L\right] \tag{3}$$

$$\text{Spleen} \quad \frac{dC_S}{dt} = \frac{1}{V_S}\left[C_P Q_S - \frac{C_S}{R_S}Q_S\right] \tag{4}$$

$$\text{Kidneys} \quad \frac{dC_K}{dt} = \frac{1}{V_K}\left[C_P Q_K - \frac{C_K}{R_K}(Q_K + K_K)\right] \tag{5}$$

where C_i is the concentration in organ *i*, *t* is time, R_i is the distribution ratio in organ *i*, Q_i is the volumetric flow rate of plasma through organ *i*, V_i is the volume of organ *i*, and K_i is the clearance rate from organ *i*. A complete list of variables and their respective descriptions can be viewed in the Nomenclature section.

Development of an additional organ compartment

Simulations conducted via MATLAB produced a quantitative analysis of the biodistribution of the nanoparticle in the previously discussed organs of a mouse as a function of time. Predetermined constants for each organ, such as blood flow rate, blood flow distribution rates through each of the organs, and organ volumes were used in the model. However, simulations of the model shown in Eqs. 2–5 showed substantial deviation from the experimental data. This can be explained by the behavior of the experimental data, which shows a violation of the conservation of the mass of drug in the body. At the time of injection ($t = 0$), theory predicts that 100% of the dose appears in the blood as a step input; furthermore, assuming only accumulation of nanoparticles in the noted four organs, as time elapses, concentration of the nanoparticles in the

Table 1 Model parameters/constants

Organ	Volume [mL]	Blood flow rate [mL/min]	Clearance rate[a] [mL/min]	Distribution ratio[a] [a.u.]	Distribution from "other" organ[a] [a.u.]
Plasma	1.70	–	–	–	–
Liver	1.30	0.75[a]	–	7.87	14.90
Kidneys	0.34	1.30	2.74	1.85	2.50
Spleen	0.10	0.09	–	1.17	8.43
Other	1.01[a]	0.78	–	10.13	–

a.u., arbitrary units.
[a]Denotes that the parameters were determined to fit the data.

blood decays on the same order of magnitude that the concentration of nanoparticles in the other organs accumulates. The clinical data supplied does not reflect this behavior. Instead, the rate of decay of nanoparticles in the blood is much faster than the rate of accumulation of the nanoparticles in the liver, spleen, and kidneys. Thus, from a physical standpoint, there must exist accumulation of the nanoparticles elsewhere, which accounts for the delay in appearance of the drug in the liver, spleen, and kidneys. Because no clinical data in other organs was collected, a new organ was introduced in the model that accounts for the loss of nanoparticles in the body, denoted "o" for "other" shown in **Figure 4**.

This new organ, in theory, should see a sharp increase in concentration after the injection of the drug, which occurs in parallel with the drop in concentration in the plasma, and should subsequently see a slow decrease over time as accumulation in the liver, spleen, and kidneys occurs. Because data shows that the plasma never sees any increase in nanoparticles after the injection, the "other" organ must be somehow connected to the liver, spleen, and kidneys such that the concentration of nanoparticles drops in the "other" organ while simultaneously increasing in the liver, spleen, and kidneys. The mass balances that were developed resemble the following:

$$\text{Plasma}\quad \frac{dC_P}{dt}=\frac{1}{V_P}\left[\left(\frac{C_L}{R_L}Q_L+\frac{C_S}{R_S}Q_S+\frac{C_K}{R_K}Q_K+\frac{C_O}{R_O}Q_O\right)-C_P(Q_L+Q_S+Q_K+Q_O)\right] \tag{6}$$

$$\text{Liver}\quad \frac{dC_L}{dt}=\frac{1}{V_L}\left[\left(C_P(Q_L-Q_S)+\frac{C_S}{R_S}Q_S+\frac{C_O}{R_{LO}}Q_O\right)-\frac{C_L}{R_L}(Q_L+Q_O)\right] \tag{7}$$

$$\text{Spleen}\quad \frac{dC_S}{dt}=\frac{1}{V_S}\left[\left(C_PQ_S+\frac{C_O}{R_{SO}}Q_O\right)-\frac{C_S}{R_S}(Q_S+Q_O)\right] \tag{8}$$

$$\text{Kidneys}\quad \frac{dC_K}{dt}=\frac{1}{V_K}\left[\left(C_PQ_K+\frac{C_O}{R_{KO}}Q_O\right)-\frac{C_K}{R_K}(Q_K+Q_O+K_K)\right] \tag{9}$$

$$\text{Other}\quad \frac{dC_O}{dt}=\frac{1}{V_O}\left[Q_O\left(C_P-\frac{C_O}{R_O}\right)\right] \tag{10}$$

Model parameters/constants

Constants in the model, such as the volume of organ and blood flow rate through each organ, are predetermined,[6,7] where only the volumetric flow rate through the liver (Q_L) was re-estimated to acquire better agreement between the model and the experiments. Because the accumulation of a significant amount of nanoparticles initially injected were unaccounted for, it is unlikely that predetermined distribution ratios and clearance rates can accurately predict nanoparticle distribution. Thus, new estimated values for these parameters were determined to describe more adequately the system at hand. Furthermore, the addition of a new organ into the model introduces four new distribution ratios, R_{LO}, R_{KO}, R_{SO}, and R_O. These parameters affiliated with the "other" organ had to be estimated as well, given that no physiological data to describe such an organ was available. A complete list of parameters and constants used in the model are listed in **Table 1**.

SENSITIVITY ANALYSES

Sensitivity analyses were conducted by perturbing each estimated parameter by a set value (±20%) and observing the system response while all other estimated parameters remained constant. Estimated parameters were considered sensitive when divergence in the simulation was observed or when a perturbation shifted the model prediction beyond the experimental error.

Acknowledgments. The authors thank Daniel Cook for his input on the model and on the drafting of the manuscript.

Author Contributions. P.S.D., M.J.G., V.K., L.S., and A.K.R. wrote the manuscript. P.S.D., V.K., and L.S. designed the research. M.J.G. and L.S. performed the research. P.S.D., M.J.G., V.K., X.J., and A.K.R. analyzed the data. P.S.D., V.K., X.J., and A.K.R. contributed new reagents/analytical tools.

Conflict of Interest. The authors declared no conflict of interest.

Study Highlights

WHAT IS THE CURRENT KNOWLEDGE ON THE TOPIC?

✓ Dex, a steroid hormone, is widely used to treat pediatric leukemia. However, prolonged exposure to high doses of Dex causes debilitating side effects in children treated for leukemia. A predictive physiologically based pharmacokinetic model has not been applied until now to optimize dosage limits for Dex in pediatric leukemia therapy.

WHAT QUESTION DID THIS STUDY ADDRESS?

✓ Is it possible to develop a valid systems biology approach to predict the pharmacokinetics of drug-encapsulated nanoparticles in mice and humans using experimental data of biodistribution in mice using labeled nanoparticles?

WHAT THIS STUDY ADDS TO OUR KNOWLEDGE

✓ The results depict consistency between model predictions and experimental data at short and long time intervals, indicating that our modeling approach can predict short- and long-term pharmacokinetic behavior of nanodrugs in biological systems.

HOW THIS MIGHT CHANGE CLINICAL PHARMACOLOGY AND THERAPEUTICS?

✓ The proposed model with parameters derived from *in vivo* data could therefore be potentially used as a tool to predict safe and effective doses for Dex and other anticancer drugs using nanoparticles in children.

Nomenclature

Volumes	**Units**	**Description**
V_P	mL	Volume of plasma
V_L	mL	Volume of liver
V_S	mL	Volume of spleen
V_K	mL	Volume of kidneys
V_O	mL	Volume of "other"
Flow rates	Units	Description
Q_L	mL min^{-1}	Flow rate through liver
Q_S	mL min^{-1}	Flow rate through spleen
Q_K	mL min^{-1}	Flow rate through kidneys
Q_O	mL min^{-1}	Flow rate through "other"
Concentrations	Units	Description
C_P	mcg mL^{-1}	Concentration in plasma
C_L	mcg mL^{-1}	Concentration in liver
C_S	mcg mL^{-1}	Concentration in spleen
C_K	mcg mL^{-1}	Concentration in kidneys
C_O	mcg mL^{-1}	Concentration in "other"
Distribution ratios	Units	Description
R_L	mcg/mcg	Distribution ratio in liver
R_S	mcg/mcg	Distribution ratio in spleen
R_K	mcg/mcg	Distribution ratio in kidneys
R_O	mcg/mcg	Distribution ratio of "other"
R_{LO}	mcg/mcg	Distribution ratio of "other" to liver
R_{SO}	mcg/mcg	Distribution ratio of "other" to spleen
R_{KO}	mcg/mcg	Distribution ratio of "other" to kidneys
Clearance rates	Units	Description
K_K	mL min^{-1}	Clearance rate from kidneys

1. Bischoff, K.B., Dedrick, R.L., Zaharko, D.S. & Longstreth, J.A. Methotrexate pharmacokinetics. *J Pharm. Sci.* **60**, 1128–1133 (1971).
2. Jones, H. & Rowland-Yeo, K. Basic concepts in physiologically based pharmacokinetic modeling in drug discovery and development. *CPT Pharmacometrics Syst. Pharmacol.* **2**, e63 (2013).
3. Rowland, M., Balant, L. & Peck, C. Physiologically based pharmacokinetics in drug development and regulatory science: a workshop report (Georgetown University, Washington, DC, 29–30 May 2002). *AAPS J.* **6**, 56–67 (2004).
4. Bischoff, K.B. Physiological pharmacokinetics. *Bull. Math. Biol.* **48**, 309–322 (1986).
5. Li, M., Al-Jamal, K.T., Kostarelos, K. & Reineke, J. Physiologically based pharmacokinetic modeling of nanoparticles. *ACS Nano.* **4**, 6303–6317 (2010).
6. Birnbaum, L. *et al.* Physiological parameter values for PBPK models. A report prepared by the International Life Sciences Institute Risk Science Institute. U.S. Environmental Protection Agency Office of Health and Environmental Assessment (1994).
7. Davies, B. & Morris, T. Physiological parameters in laboratory animals and humans. *Pharm. Res.* **10**, 1093–1095 (1993).
8. Hu, Z.Y., Lu, J. & Zhao, Y. A physiologically based pharmacokinetic model of alvespimycin in mice and extrapolation to rats and humans. *Br. J. Pharmacol.* **171**, 2778–2789 (2014).
9. Shah, D.K. & Betts A.M. Towards a platform PBPK model to characterize the plasma and tissue disposition of monoclonal antibodies in preclinical species and human. *J. Pharmacokinet. Pharmacodyn.* **39**, 67–86 (2012).
10. Horton, S., Tuerk, A., Cook, D., Cook, J. & Dhurjati, P. Maximum recommended dosage of lithium for pregnant women based on a PBPK model for lithium absorption. *Adv. Bioinformatics* **2012**, 352729 (2012).
11. Chou, L.Y. & Chan, W.C. Fluorescence-tagged gold nanoparticles for rapidly characterizing the size-dependent biodistribution in tumor models. *Adv. Healthc. Mater.* **1**, 714–721 (2012).
12. Hainfeld, J.F., Slatkin, D.N., Focella, T.M. & Smilowitz, H.M. Gold nanoparticles: a new X-ray contrast agent. *Br. J. Radiol.* **79**, 248–253 (2006).
13. Cheng, Y., Meyers, J.D., Broome, A.M., Kenney, M.E., Basilion, J.P. & Burda C. Deep penetration of a PDT drug into tumors by noncovalent drug-gold nanoparticle conjugates. *J. Am. Chem. Soc.* **133**, 2583–2591 (2011).
14. Loginova, Y.F. *et al.* Biodistribution of intact fluorescent CdSe/CdS/ZnS quantum dots coated by mercaptopropionic acid after intravenous injection into mice. *J. Biophotonics* **5**, 848–859 (2012).
15. Paciotti G.F. *et al.* Colloidal gold: a novel nanoparticle vector for tumor directed drug delivery. *Drug Deliv.* **11**, 169–183 (2004).
16. Lin, P. *et al.* Computational and ultrastructural toxicology of a nanoparticle, Quantum Dot 705, in mice. *Environ. Sci. Technol.* **42**, 6264–6270 (2008).
17. Krishnan, V. *et al.* Dexamethasone-loaded block copolymer nanoparticles induce leukemia cell death and enhance therapeutic efficacy: a novel application in pediatric nanomedicine. *Mol. Pharm.* **10**, 2199–2210 (2013).
18. Gaynon, P.S. & Carrel, A.L. Glucocorticosteroid therapy in childhood acute lymphoblastic leukemia. *Adv. Exp. Med. Biol.* **457**, 593–605 (1999).
19. Stuart, F.A., Segal, T.Y. & Keady, S. Adverse psychological effects of corticosteroids in children and adolescents. *Arch. Dis. Child.* **90**, 500–506 (2005).
20. Krishnan, V. & Rajasekaran, A.K. Clinical nanomedicine: a solution to the chemotherapy conundrum in pediatric leukemia therapy. *Clin. Pharmacol. Ther.* **95**, 168–178 (2014).
21. Tan, J., Thomas, A. & Liu, Y. Influence of red blood cells on nanoparticle targeted delivery in microcirculation. *Soft Matter* **8**, 1934–1946 (2011).
22. Bazemore, A.W. & Smucker, D.R. Lymphadenopathy and malignancy. *Am. Fam. Physician* **66**, 2103–2110 (2002).
23. Murray, R.A., Thom, G., Gardner, R.V. & Craver, R.D. Infant acute lymphoblastic leukemia: a 20-year children's hospital experience. *Fetal Pediatr. Pathol.* **27**, 197–205 (2008).

Supplementary information accompanies this paper on the *CPT: Pharmacometrics & Systems Pharmacology* website (http://www.wileyonlinelibrary.com/psp4)